Research Paper

High resolution paleo-environmental changes during the Sapropel 1 in the North Ionian Sea, central Mediterranean

Helena Checa,[1,2] (ID) Giulia Margaritelli,[3]
Leopoldo D Pena,[2] Jaime Frigola,[2]
Isabel Cacho,[2] Roberto Rettori[1] and Fabrizio Lirer[4]

Abstract

High-resolution paleoceanographic reconstruction of surface water properties during the most recent Sapropel event (S1) has been carried out by means of quantitative analyses of planktonic foraminiferal assemblages, planktonic foraminiferal oxygen isotopes ($\delta^{18}O$) and XRF elemental data from a 655 m depth core recovered in the North Ionian Sea. The results show that the S1 interval presents two distinctive warm phases (S1a and S1b), separated by a cold interruption event (S1i). High resolution faunal and geochemical analyses allow to identify two sub-phases within S1a interval, the oldest one has similar characteristics to S1b interval while the youngest sub-phase has less stratified surface waters with relatively lower nutrient content. The high abundance of *Globigerinoides ruber* white variety opposite to the low percentages of *Neogloboquadrina pachyderma* during the pre-S1 phase suggests that the onset of surface waters stratification occurred prior to the beginning of Sapropel deposition, acting as a pre-conditioning phase. Paleo-productivity proxies indicate that the deposition of S1 initiated after an increase in nutrient content, potentially related to increased fluvial inputs. Based on the integrated ecological interpretation of our records we argue that S1a and S1b are characterized as warm, stratified and nutrient rich surface waters in the Ionian Sea, while proxies related to oxygen content indicate dysoxic deep waters linked to a combination of the high nutrient content and stratified water column. The S1 interruption phase is characterized by the entrance of colder waters that caused mixing of the stratified water column and re-ventilation of the deep dysoxic waters.

Introduction

The deposition of dark-coloured, organic-rich sediment layers (Sapropels) in the eastern Mediterranean Sea have been described and characterized by several studies (Calvert et al., 2001; Casford et al., 2002, 2003; De Lange et al., 1999, 2008; Filippidi et al., 2016; Geraga et al., 2008; Giamali et al., 2019; Kallel et al., 2000; Kontakiotis, 2016; Kontakiotis et al., 2009, 2013; Kotthoff et al., 2008; Mélières et al., 1997; Plancq et al., 2015; Rohling, 1994; Rohling et al., 1997, 2015; Siani et al., 2010; Tesi et al., 2017;). However, there is a lack of consensus on the precise mechanisms and the exact sequence of climatic and oceanographic events that lead to the formation of Sapropels. It is generally accepted that Sapropels are the result of complex interactions between regional climatic, oceanographic and biogeochemical processes as a response to shifting global climate patterns (De Lange et al., 2008; Grimm et al., 2015; Le Houedec et al., 2020; Mercone et al., 2000, 2001; Rohling et al., 2015; Tachikawa et al., 2015; Vadsaria et al., 2019). Sapropel 1 (S1) is the only sapropel event that appears during Early-Mid-Holocene (interglacial period), between 10.8 ± 0.4 and 6.1 ± 0.5 kyrs BP (De Lange et al., 2008; Incarbona et al., 2019). General consensus suggests that the deposition of S1 was caused by the combination of three main factors. First, the freshening and stratification of Mediterranean surface waters, both from low salinity Atlantic inflow through Gibraltar

Strait as well as from increased river runoff (Geraga et al., 2010; Kontakiotis, 2016; Kontakiotis et al., 2009, 2013; Mojtahid et al., 2019) resulting from northward shifting and intensification of the African monsoon (De Lange et al., 1999, 2008; Grant et al., 2016; Hennekam et al., 2014; Rohling, 1994; Rohling et al., 1997, 2015). Second, the increased river discharge was accompanied by a resupply of land-derived nutrients to the surface ocean, followed by enhanced primary productivity and export of organic

[1]Dipartimento di Fisica e Geologia, Fac. di Geologia. Università degli studi di Perugia, Italy
[2]GRC Geociències Marines, Department de Dinàmica de la Terra i de l'Oceà, Facultat de Ciències de la Terra, Universitat de Barcelona, Spain
[3]Istituto di Ricerca per la Protezione Idrogeologica (IRPI-CNR), Consiglio Nazionale delle Ricerche, Italy
[4]Istituto di Scienze Marine (ISMAR)-CNR - Sede di Napoli, Consiglio Nazionale delle Ricerche, Calata Porta di Massa, Interno Porto di Napoli, Italy

Corresponding author:
Helena Checa, Dipartimento di Fisica e Geologia, Facoltà di Geologia, Università degli studi di Perugia, Via Alessandro Pascoli, s.n.c Perugia, 06123, Italy.
Email: helena.checasanchez@studenti.unipg.it
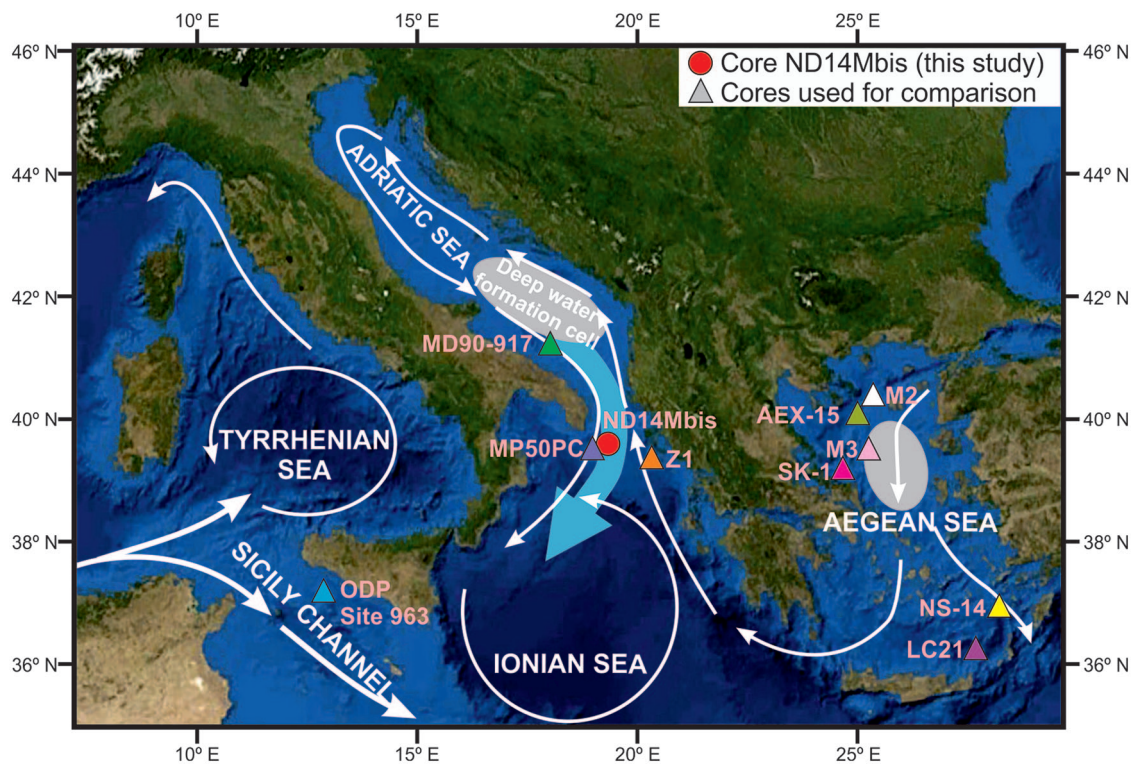
Figure 1. Map of the study area showing the modern surface (white arrows) and deep (blue arrow) circulation patterns based on Rohling et al. (2009), and also core ND14Mbis location. Other reference core sites used in the text for comparison (LC-21, Casford et al. (2002) and Rohling et al. (2002); ODP Site 963, Sprovieri et al. (2003); M2 and M3, Roussakis et al. (2004); Z1, Geraga et al. (2008); MD90-917, Siani et al. (2010); MP50PC, Filippidi et al. (2016) and Filippidi and De Lange (2019); SK-1 and NS-14, Kontakiotis (2016); AEX-15, Giamali et al. (2019) are also shown.

matter to the bottom of the basin (De Lange et al., 2008; Rohling and Gieskes, 1989; Rohling et al., 1997). Third, enhanced surface ocean stratification also resulted in reduced ventilation rates of the deep waters through deep water convection (i.e. reduction in dissolved oxygen export) that in turn favoured the preservation of the organic matter due to the establishment of dysoxic conditions (Abu-Zied et al., 2008; De Lange et al., 1999, 2008; Drinia et al., 2016; Grimm et al., 2015; Le Houedec et al., 2020; Louvari et al., 2019; Rohling et al., 2015; Schmiedl et al., 2010). All these factors together could contribute to the formation of the Eastern Mediterranean (EMED) S1 layer.

Several studies have shown that S1 can be subdivided into two distinctive phases (S1a and S1b) separated by an interruption phase (Giamali et al., 2019; Kontakiotis, 2016; Myers and Rohling, 2000; Rohling et al., 1997; Rohling and Pälike, 2005; Triantaphyllou et al., 2009). While both S1a and S1b were periods of warm, stratified waters with dysoxic bottom conditions, the interruption period (S1i) was characterized by the arrival of cold surface waters, which favoured vertical mixing and enhanced re-ventilation of the EMED deep waters (De Rijk et al., 1999; Incarbona et al., 2019; Myers and Rohling, 2000; Rohling et al., 1997, 2015; Rohling and Pälike, 2005; Schmiedl et al., 2010;). The onset and the end of S1 deposition throughout the eastern Mediterranean Sea appears to not have been synchronous (10.8 ± 0.4–6.1 ± 0.5 kyrs BP; De Lange et al., 2008), independently of the water depth of deposition (De Lange et al., 2008; Klein et al., 2000; Schmiedl et al., 2010). However, although S1 has been characterized in many different locations through the Eastern Mediterranean, there is a lack of information available on the northern part of the central Mediterranean basin (Adriatic and Ionian Seas).

This study is focused on the study of the expression of S1 in the northern part of the Ionian Sea, which is a key area for understanding the Mediterranean thermohaline circulation (MedTHC) system. In this sense, the Ionian Sea acts as an important gateway

between the Adriatic Sea and the rest of the Mediterranean, where water exchange occurs both at surface and intermediate-deep levels. Surface and intermediate waters from the Ionian Sea enter the Adriatic Sea forming a cyclonic gyre, while Adriatic Deep waters (ADW) overflow to the Ionian Sea (Cushman et al., 2001; Manca et al., 2003). These complex interactions between the Adriatic and the Ionian Sea make this study area a key gateway zone. With the objective of understanding the hydrographic changes that lead to the Sapropel formation in the study area, we present the first high resolution dataset with precise chronology for the North Ionian Sea, containing proxy records from planktonic foraminifera assemblages, stable isotopes ($\delta^{18}O$) and bulk XRF elemental composition of sediments. Although S1 has been previously defined as having two main phases (S1a and S1b), their characterization has never been done at very high resolution, thus lacking the possibility of identifying centennial or even decadal variability within this time interval. Thus, the final goal of this study is the understanding of the hydrographic changes that lead to the Sapropel S1 formation in the central Mediterranean at very high resolution (centennial or decadal) along with the reconstruction of the oceanographic conditions and climate variability over this time interval.

Study area

The Mediterranean is a semi-enclosed Sea divided by two main basins, the western and eastern Mediterranean, separated by the Sicily channel (Figure 1). Its reduced spatial scale, partial isolation and marginal configuration make the Mediterranean Sea an excellent "natural laboratory" acting as an amplifier, where climatic and oceanographic processes can be studied with a better signal to noise ratio compared to the open ocean (Antonarakou et al., 2019; Cacho et al., 2001; Kontakiotis, 2016; Rohling et al., 2015). The Mediterranean Sea sediments have proved to be an excellent archive where climatic events can be recorded (i.e. Bazzicalupo et al., 2020; Koutrouli et al., 2018; Lirer et al., 2013; Margaritelli

et al., 2018). Typically, high sedimentation rates during the Holocene represent one of the most powerful tools to monitoring the climate evolution by amplifying the climatic signals over the Holocene (Antonarakou et al., 2018; Cacho et al., 2001; Giamali et al., 2019; Louvari et al., 2019; Marino et al., 2009).

The study core ND14Mbis is located at the north-east end of the Ionian Sea. The Ionian Sea waters are connected with the Adriatic Sea on the north by the Otranto strait, with the Aegean Sea on the east and the Tyrrhenian Sea on the west through the Sicily Channel. Adriatic deep waters (ADW) typically overflow through the Otranto strait and contribute as one of the main sources and precursors of Eastern Mediterranean Deep Waters (EMDW) (Manca et al., 2003) (Figure 1). Across the Sicily Channel, a surface layer of strongly Modified Atlantic Water (MAW) enters the Levantine basin from the western Mediterranean (Figure 1). That surface water inflow is balanced out through the outflow of intermediate (Levantine Intermediate Water, LIW) and deep (EMDW) waters into the Tyrrhenian Sea (Garcia-Solsona et al., 2020; Manca et al., 2003) (Figure 1).

The Adriatic Sea typically presents lower surface salinities than the rest of the Mediterranean, mostly due to large fresh water discharge from rivers (e.g. Po River, Ofanto River), and it collects up to a third of the total annual fresh water discharge into the Mediterranean, thus acting as a dilution basin (Manca et al., 2003; Özsoy et al., 1989). In the southern part of the Adriatic Sea, there is a deep water convection cell that forms dense waters (ADW) (Cushman et al., 2001; Özsoy et al., 1989) (Figure 1). The formation of this water mass starts with the pre-conditioning of surface waters with sustained cold, dry north-easterly winds. As a result, buoyancy loss of surface waters through intense cooling and evaporation result in the establishment of a deep water convection system. The ADW is formed when this denser and cold waters flows towards the deep South Adriatic basin and mixes with LIW, a relatively warm and salty water mass. The result of this mixing is a denser water mass (the ADW) that spills over into the Ionian Sea through the Otranto strait and sinks into the deep basin becoming the primary source of EMDW (Cushman et al., 2001; Özsoy et al., 1989, Figure 1). Being a dilution basin, the Adriatic Sea exports relatively fresh surface waters to the Ionian Sea which is compensated by the inflow of warmer and saltier waters from the eastern Mediterranean through the surface and intermediate water layers (Cushman et al., 2001). The surface ocean currents flow counter-clockwise from the Strait of Otranto, passing by the eastern coast and then southward to the strait by the western (Italian) coast (Figure 1).

Material and methods

This study focuses on the S1 sedimentary sequence of the gravity core ND14Mbis, recovered during the Next-Data 2014 expedition on board of the Italian Vessel R/V Urania-CNR. The core is located at the north-eastern part of the Ionian Sea (39°35′53,94″N, 18°47′40,48″E, 655 m depth) (Figure 1) along the exit pathway of deep waters from the Adriatic Sea into the Ionian Sea. Core length is 332 cm and the studied interval is located between the interval 80–150 cm, which comprises the pre-Sapropel, the Sapropel layer (between 105 and 126 cm) and the post-Sapropel intervals. The Sapropel interval is characterized by two dark layers of 11 and 5 cm respectively, interbedded by a light interval of 5 cm, above the Sapropel unit, we can see a 2 cm light dark layer (between 103 and 105 cm) lithologically similar to the sapropel (Figure 2a). For this study, the entire core was sampled at 1 cm resolution.

Stable isotopes

We have measured oxygen stable isotopes ($\delta^{18}O$) on *Globigerinoides ruber* white variety, through S1 interval at 1 cm resolution (71 samples). Between 10 and 15 specimens of *G. ruber* white
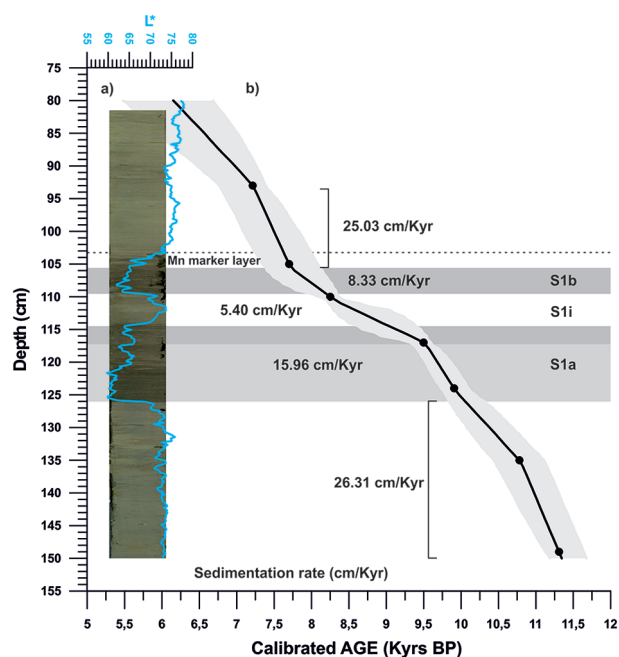
Figure 2. (a) High resolution digital image of core ND14Mbis and lightness values (L*) (blue line) acquired with the high-resolution colour line scan camera of Avaatech XRF core scanner at the CORELAB laboratory of the University of Barcelona. Different phases within sapropel 1 are identified with black boxes (S1a, S1i and S1b) and the Mn marker layer has been highlighted with a dotted line. (b) Age model of core ND14Mbis around Sapropel 1 time interval (marked in grey). Age-depth correspondence is marked with a white line while the light grey cloud represents age uncertainties (2 sigma). Corresponding sediment accumulation rates are also shown.

(>150 μm) were picked. The samples were crushed and sonicated in methanol to remove fine-grained detrital particles. These analyses were performed with a mass spectrometer Finnigan MAT 252 fitted with a carbonate preparation line (Kiel device), at the University of Barcelona (CCiT-UB). The estimated external reproducibility is typically <0.05‰ for $\delta^{18}O$. Calibration to Vienna Pee Dee Belemnite (VPDB) was carried out following NBS-19 standards (Coplen, 1996).

X-ray fluorescence (XRF)

Bulk elemental geochemical composition of core ND14Mbis was measured with an Avaatech XRF core scanner at the CORELAB laboratory of the University of Barcelona. The sediment core was measured at 1 cm resolution with excitation conditions of 10 kV, 0.5 mA and 10 s for major elements (Al, Si, S, K, Ca, Ti, Mn, Fe), 30 kV, 1.0 mA, 30 s with a Pd-thick filter for Br, Rb, Sr and Zr, and 50 kV, 1.0 mA, 30 s and a Cu filter for Ba. In addition, the core section corresponding to S1 interval (dark layers in Figure 2a) was measured at 2 mm resolution with excitation conditions of 10 kV, 1.0 mA and 10 s, 30 kV, 1.4 mA, 45 s with a Pd-thick filter, and 50 kV, 1.4 mA, 45 s and a Cu filter. The relative abundance of the elements of interest is shown as elemental ratios normalized to Al as a way to avoid the dilution effect that happens to some elements (Calvert and Pedersen, 2007).

Planktonic foraminiferal assemblages

The planktonic foraminiferal analysis was realized on a total of 71 samples with 1 cm resolution. The bulk sediment samples were dried at 60°C in the oven and then wet sieved through a 63 μm mesh to separate sand and clay fractions. Quantitative planktonic foraminiferal analysis was done in the >150 μm fraction. For each

Table 1. (a) Summary of the main ecological habitats of some planktonic foraminifera taxa following Cita et al. (1977); Hemleben et al. (1989); Pujol and Vergnuad-Grazzini (1995); Sprovieri et al. (2003); Kontakiotis et al. (2017). (b) List of tie points with corresponding dated species. Absolute dates (AMS[14]C) are indicated with their corresponding uncertainties (two sigma) and the calibrated ages obtained, expressed as years Before Present (BP). Sedimentation rates are shown as cm/kyr.

(a) Specie	Ecological preference
Globigerina bulloides	Cold waters, upwelling areas after phytoplankton and zooplankton blooms.
Globigerinita glutinata	Cold, well-mixed, high nutrient waters. Opportunistic response to increases on nutrients. Areas with continental runoff.
Globigerinoides elongatus	Depending of the summer thermocline during oligotrophic conditions.
Globigerinoides ruber white variety	Shallow dwelling species. Warm, oligotrophic, salty, well stratified surface waters.
Globigerinoides ruber pink variety	Shallow dwelling species. Warm, salty, well stratified surface waters with a high nutrient content.
Globigerinoides sacculifer	Shallow, warm, low salinity, well stratified euphotic zone and oligotrophic mixed layer.
Globigerinoides quadrilobatus	
Globorotalia inflata	Cold and deep mixed layer. No deep chlorophyll maximum.
Globorotalia scitula	Cold waters.
Turborotalita quinqueloba	Cold, high productivity surface waters. Continental run-off.
Globigerinella siphonifera	Warm upwelling waters.
Orbulina spp.	Warm surface waters.
Neogloboquadrina dutertrei	Cold waters with high productivity and deep chlorophyll maximum.
Neogloboquadrina pachyderma	Cold, deep-dwelling and high productivity. Lives close or below the thermocline. Deep chlorophyll maximum at the base of the euphotic layer.
Globorotalia truncatulinoides	Cold waters with strong deep mixing. High nutrient. No deep chlorophyll maximum.
P/B ratio	Productivity variations or terrigenous input (dilution effects).

(b) CORE ND14Mbis

Depth (cm)	Dated specie	Uncorrected AMS [14]C (yrs BP)	Calibrated (yrs BP) with Rstudio	Age uncertainties interval (yrs BP)	Sedimentation rate (cm/Kyr)
30	*G. ruber* + *G. bulloides*	2422 ± 26	2075	1940.2–2258	12.62
93	*G. ruber* + *G. bulloides*	6777 ± 25	7215.9	6768.3–7391.9	21.93
105	*G. ruber*	6857 ± 24	7702.9	7343.7–8090	14.04
110	*G. ruber*	7803 ± 27	8254	8097–8374.1	7.10
117	*G. ruber*	8876 ± 30	9501.8	9320.6–9602.6	13.28
124	*G. ruber*	9110 ± 34	9911.1	9734.7–10105.8	14.58
135	*G. ruber* + *G. bulloides*	10170 ± 34	10785.7	10442.4–11114.6	20.83
149.5	*G. ruber* + *G. bulloides*	10269 ± 33	11333.4	11168.9–11663.4	27.47
210	*G. ruber*	12419 ± 53	13969.4	13748.8–14247.7	21.69
273	*G. ruber* + *G. bulloides*	14675 ± 50	17417.3	17122.8–17745.3	15.67

sample a number between 200 and 300 individuals were counted and identified following morphotype-specific (Kontakiotis et al., 2017) and/or specialized taxonomical concepts and ecological inferences (Hemleben et al., 1989; Pujol and Vergnaud-Grazzini, 1995), summarized in Table 1a. Species with phylogenetic affinities and similar ecological characteristics were counted together and grouped to better interpret distribution patterns.

Some planktonic species have been grouped as follows: *Globigerina bulloides, Globigerinita glutinata, Globigerinoides elongatus, Globigerinoides ruber* divided in the white and the pink varieties, *Globigerinoides quadrilobatus* which includes *Globigerinoides trilobus* and *Globigerinoides sacculifer, Globorotalia inflata, Globorotalia scitula* distinguishing between left and right coiling, *Turborotalita quinqueloba, Globigerinella siphonifera* which includes *Globigerinella calida, Orbulina* spp. which includes *Orbulina universa* and *O. suturalis, Neogloboquadrina dutertrei* and, finally, *Neogloboquadrina pachyderma* and *Globorotalia truncatulinoides* distinguishing in both between left and right coiling. These species are represented in percentages of the total assemblage. In order to characterize environmental changes, the planktonic/benthic foraminifera ratio (P/B ratio) was also calculated and plotted.

Age model

The age model of core ND14Mbis is based on ten radiocarbon (^{14}C) AMS measurements, seven of which were strategically selected along the S1 interval, including the pre- and post- intervals (Figure 2b). 3–6 mg per sample of monospecific *G. ruber* white variety (and *G. bulloides* in some cases) were handpicked from the >150 μm fraction (Table 1b). Samples were graphitized at the Godwin Laboratory for Palaeoclimate Research of the University of Cambridge (UK) following the protocol described on Freeman et al. (2016) and analysed at the [14]CHRONO Centre of the Queen's University of Belfast (UK). Radiocarbon ages were calibrated using MARINE13 calibration curves (Reimer et al., 2013) to account for global marine reservoir ages and to obtain calendar ages (cal yr BP), age correction for regional reservoir effects (ΔR) was not applied due to the lack of reliable estimates. The age model was constructed using the Bayesian statistics software Bacon with the statistical package R (Blaauw and Christien, 2011). Hereafter, the ND14Mbis calibrated ages are reported as kyrs.

Based on the constructed age model, the sedimentation rates were estimated to be ~26.3 cm/kyr for the pre-Sapropel period, ~15.9 cm/kyr for the S1a, ~5.4 cm/kyr for the S1i, ~8.3 cm/kyr for the S1b and ~25 cm/kyr for the post-Sapropel period (Table 1b). This is equivalent to a temporal sampling resolution of 38–185 year per sample, therefore allowing sub-millennial events in the sedimentary record to be inferred. In addition, focusing only on Sapropel S1 deposition, the mean sedimentation rate of the study core (~10 cm/kyr) is almost comparable with the sedimentation rate of other Sapropel S1 Mediterranean records, independently of the water depth, as follows: North

Ionian Sea (~10 cm/kyr, Filippidi et al., 2016), North-east
Ionian Sea (~5.5 cm/kyr, Geraga et al., 2008), Adriatic Sea
(~20 cm/kyr, Mercone et al., 2000; Siani et al., 2010), South
Aegean Sea (~10.3 cm/kyr, Casford et al., 2002), North Aegean
Sea (~15.4 cm/kyr, Roussakis et al., 2004 and 17,3 cm/kyr Gia-
mali et al., 2019) and Eastern Levantine basin (~20 cm/kyrs,
Cornuault et al., 2018). On the other hand, our average sedi-
mentation rates during the S1 are significantly different from
other core sites with exceptionally high sedimentation rates in
the North (67.6 cm/kyr, Kontakiotis, 2016) and South Aegean
(~37.5 cm/kyr, Kontakiotis, 2016) Sea records. These differ-
ences in sedimentation rate from different sites of the Mediter-
ranean could be related to several factors such as continental
input, regional oceanography, water depth, deep currents lateral
sediment transport, etc.

Results

Stable isotopes

The $\delta^{18}O_{G.ruber}$ signal shows relatively heavy isotopic ratios
(1.25–2.35‰) at the base of the studied interval (11.3–6 kyrs BP)
followed by a trend towards lighter $\delta^{18}O$ values that culminates at
the onset of S1a (10 kyrs BP) with relatively light values (–0.22–
0.95‰) (Figure 3a). This record has been compared with nearby
deep-sea cores (Filippidi and De Lange, 2019; Geraga et al.,
2008; Rohling et al., 2002 and Siani et al., 2010; Figure 3). To
prevent age model discrepancies between core sites in the data
comparison we have recalculated the radiocarbon age models for
the published $\delta^{18}O_{G.ruber}$ records following the same Bayesian age
model approach adopted for the study core (cf. section 3.4). The
comparison of the recalibrated stable isotope G. ruber records
shows that in the study core (ND14Mbis) $\delta^{18}O$ reaches the lighter
interglacial values (–0.22–0.95‰) at 10 kyrs BP (Figure 3a), in
Filippidi and De Lange (2019) at 10 kyrs BP (north Ionian Sea,
Figure 3c), in Geraga et al. (2008) at 9.5 kyrs BP (north eastern
Ionian Sea, Figure 3b), in Siani et al. (2010) at 9 kyrs BP (South
Adriatic Sea, Figure 3d) and in Rohling et al. (2002) at 9.5 kyrs
BP (South Aegean Sea, Figure 3e). All these records, show rela-
tively constant $\delta^{18}O$ values around –0.3–1.2‰ throughout the
Early Holocene.

XRF analysis

Sapropel layers in sediments are typically expressed as distinct
dark coloured layers, sometimes laminated and enriched in
organic carbon. This feature makes for an easy recognizable trait
of Sapropel layers. The 37 cm-length interval that was analysed at
a higher resolution corresponds to these dark layers that can be
seen at Figure 2a. We used the lightness values (L*) obtained
from the high-resolution images of the sediments (taken with the
Avaatech XRF core scanner) to identify the Sapropel unit and its
interruption more precisely (Figure 2a). The marked decrease in
the lightness values observed in this section marks the Sapropel
layers on the core (Figures 4a and 5a). It has been shown at other
Sapropel layers that dark colour bands are often slightly thicker
than the interval defined by the organic carbon (De Lange et al.,
1999). In our study core we clearly find a light dark coloured 2 cm
thick layer (between 103 cm and 105 cm) above the defined end of
the sapropel unit based on our proxies, with a diffuse upper
boundary and a relatively abrupt colour transition at its lower
boundary (Figure 2a).

XRF elemental ratios such as Ba/Al and S/Al show particu-
larly abrupt changes through S1a and S1b intervals, synchronous
to lowest values of lightness record (Figures 4 and 5). During S1i,
all these elemental ratios recover back to similar values than dur-
ing pre-Sapropel times. After 7.7 kyrs BP (end of Sapropel depo-
sition), all proxies recover their pre-Sapropel values again.
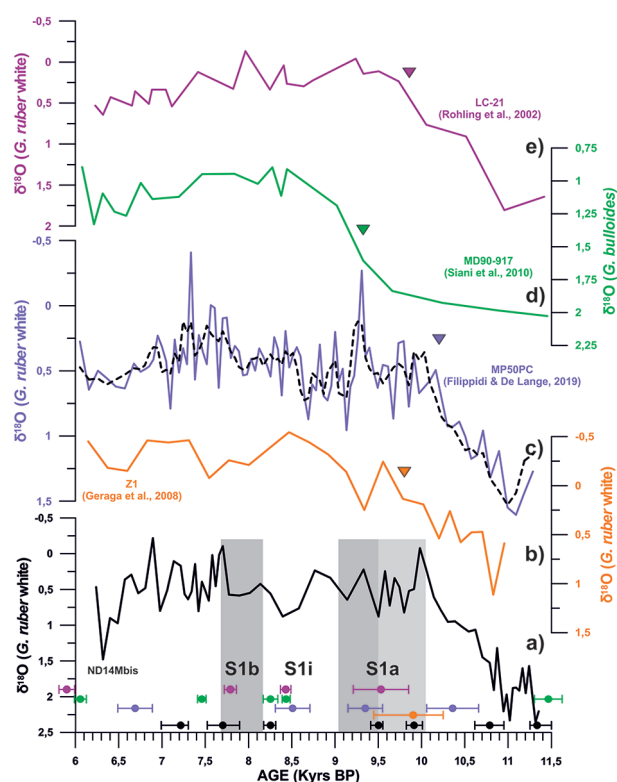
Figure 3. $\delta^{18}O_{G.ruber}$ data of core ND14Mbis represented in black,
compared to $\delta^{18}O_{G.ruber}$ data from the north Ionian Sea of core Z1
(in orange, Geraga et al., 2008), core MP50PC (in purple and in
black the mean values, Filippidi and De Lange, 2019) and the South
Aegean Sea core LC-21 (in pink, Casford et al., 2002), and
$\delta^{18}O_{G.bulloides}$ data from core MD90-917 (in green, Siani et al., 2010),
from the Adriatic Sea. Black, orange, purple, green and pink dots
correspond to each tie point used in the age model of each core.
The orange, purple, green and pink triangles correspond to the age
of the beginning of the S1 deposition according to each author. The
grey bars represent the S1a and S1b phase time intervals.

Planktonic foraminiferal assemblages

The relative percentage abundance of the most significant plank-
tonic foraminiferal species recovered in core ND14Mbis between
11.5 and 6 kyrs BP is displayed in Figure 6. Over the studied time
interval, the planktonic foraminifera were relatively abundant and
well preserved. The planktonic foraminiferal assemblage was
dominated by G. ruber white variety, G. inflata and N. pachy-
derma (right and left coiling), reaching abundances of 68.2, 42.3,
and 30.6%, respectively.

The planktonic foraminifera G. ruber pink, G. siphonifera, G.
quadrilobatus gr. and O. universa describe similar trends with
high abundance values mainly during S1a and S1b (Figure 6).
Conversely, they present lower values, before and after these two
intervals, as well as during S1i (from 9 to 8.2 kyrs BP). G. ruber
white has a distinctive behaviour with respect to the others, show-
ing an earlier onset in the abundance increase at 11 kyrs BP and
reaching its maximum peak at 10.3 kyrs BP (Figure 6a). At this
point, G. ruber white abundance starts a decreasing trend until it
reaches its lower values at 9 kyrs BP (end of S1a), while other
warm water species (G. ruber pink, G. siphonifera and O. uni-
versa) present high abundance values. G. ruber white recovers
high abundance values during S1b, presenting a similar trend to
that of the rest of the warm water species, but with lower abun-
dances than those recorded during S1a. Contrarily, G. ruber pink
warm species resembles the same trend but presents a relative
maximum peak at 8.9–8.8 kyrs BP (Figure 6b), when G. ruber
white, G. siphonifera, G. quadrilobatus and O. universa were
characterized by low relative abundances.
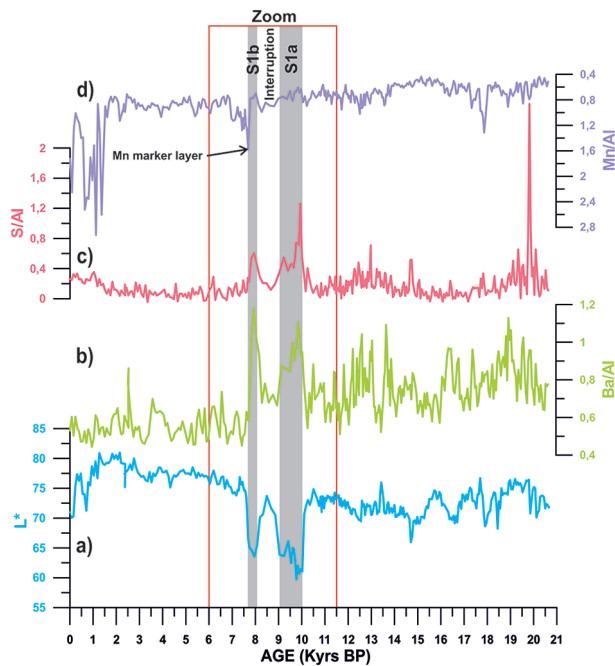
Figure 4. Records from core ND14Mbis of (a) lightness (1 cm resolution), (b) Barium/Aluminium ratio (Ba/Al), (c) Sulphur/Aluminium ratio (S/Al), and (d) Manganese/Aluminium ratio (Mn/Al). The red box represents the study period around sapropel 1, between 6 and 11.5 kyrs BP, and the grey bars mark S1a and S1b phases.
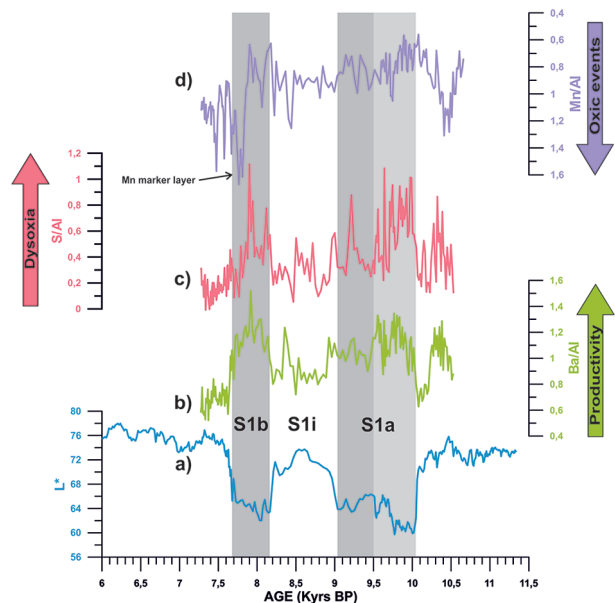
Figure 5. High-resolution (2 mm) XRF records from core ND14Mbis. (a) lightness, (b) Barium/Aluminium ratio (Ba/Al), (c) Sulphur/Aluminium ratios (S/Al), and (d) Manganese/Aluminium ratio (Mn/Al). This data corresponds to the studied period marked in red on Figure 5. Grey bars represent the S1a and S1b phase time intervals, while light grey bar shows the subdivision of S1a.

G. inflata presents a mean value of 7% in abundance during S1a and S1b phases, and increases in abundance to a mean value of 11.5% during S1i interval. With the ending of the Sapropel event (7.7 kyrs BP), *G. inflata* increases significantly reaching mean values of 25.8% (Figure 6g). *N. pachyderma* shows high relative abundances (15–31%) from 11.3 to 11 kyrs BP, then it starts a decreasing trend to 10.3 kyrs BP, in phase with *G. ruber* white increase (Figure 6a and 6h). From 10.3 kyrs BP and during

S1a, *N. pachyderma* documents its lower values (0.3–1.4%), while during the S1i interval it documents a slightly increase in abundance to mean values of 3.5%. After the end of the Sapropel event, at 7.7 kyrs BP, the percentages of *N. pachyderma* show a marked increase in abundance to 22% (Figure 6h). *G. scitula* shows a peak of abundance ranging between 0 and 3.4% during the pre-Sapropel period, followed by its disappearance at the onset of S1a (10 kyrs BP) (Figure 6). Similar to *N. pachyderma*, *G. scitula* also presents a slight increase in abundance (0–2.2%) during S1i and during the post-Sapropel record (mean values of 2.2%). *G. truncatulinoides* shows peaks of abundance (mean values of 4.5%) during the pre-Sapropel period and then it abruptly disappears at 10.1 kyrs BP, at the onset of S1a (Figure 6i).

G. quadrilobatus gr. has a continuous distribution pattern with values ranging 0.5–8.5% with a prominent peak (27%) at 8 kyrs BP (Figure 6). *G. glutinata* shows very low abundances during S1a and S1b (2–10.3%) however, during S1i and between 9.5 and 8.2 kyrs (final part of S1a), this species has two increments in abundance of 10–20%. At 7.7 kyrs, with the end of the Sapropel period, *G. glutinata* shows a progressive increase in abundance reaching values of 35% (Figure 6c).

The P/B ratio shows an abrupt increase from values of 50–79%, during the pre-Sapropel phase, to 98.8% during S1a and 100% during S1b. It presents a slight reduction during S1i down to 75.8–91.2%. After 7.7 kyrs BP (at the end of the Sapropel interval deposition), the P/B ratio values decrease to 85.5–92%. When comparing the P/B ratio values during the pre-Sapropel period (before 10 kyrs BP) with the post-Sapropel period (after 7.7 kyrs BP), it can be determined that the P/B ratio after the Sapropel resulted higher than the pre-Sapropel one (Figure 6k).

Discussion

A combined approach based on the integration of different paleoclimatic proxy signals (L*, planktonic foraminiferal assemblages, $\delta^{18}O$ records and XRF data) was used to identify and characterize S1 within a robust chronological constrain (Figure 7). In particular, we identified the following phases: S1a (10–9 kyrs BP), an interruption phase or S1i (9–8.2 kyrs BP), and S1b (8.2–7.7 kyrs BP). We defined the onset of the Sapropel taking as reference the first abrupt decrease of the L* signal (Figures 4a and 5a), associated with the disappearance of the planktonic foraminifera *G. truncatulinoides* (Figure 7d), at 10 kyrs BP. The end of S1 interval occurs at 7.7 kyrs BP, when L* values increase again.

Pre-Sapropel interval: pre-S1 (11.3–10 kyrs BP)

The time interval before S1 deposition (pre-S1) was a period characterized by a series of hydrographic changes in surface water conditions that acted as pre-conditioning factors for the S1 deposition in the Ionian Sea. This period corresponds to the onset of the Holocene after the deglaciation period (dated at 11.7 kyrs BP, Walker et al., 2018). This suggested paleoceanographic framework can be confirmed by the $\delta^{18}O$ data shown in Figure 7h.

$\delta^{18}O_{G.ruber}$ data of our study core shows a 2.2‰ transition interval from heavy to light values during the pre-Sapropel interval (11.3–10 kyrs BP), corresponding to the global sea level rise after the YD event (Grant et al., 2016) followed by relatively stable and light $\delta^{18}O_{G.ruber}$ values during the Holocene (Figure 7h). The pattern of our study record is comparable to other $\delta^{18}O$ records in the Eastern Mediterranean basin (Figure 3). However, we find that our light $\delta^{18}O$ values are achieved during the pre-S1, at 10 kyrs BP, while on the other sites light isotopic values happened at the beginning of S1 deposition; on the North Ionian record (Filippidi and De Lange, 2019) at 10 kyrs BP, on the North-eastern Ionian record (Geraga et al., 2008) at 9.5 kyrs BP, on the Southern Aegean Sea record (Rohling et al., 2002) at 9.5 kyrs BP and on the South
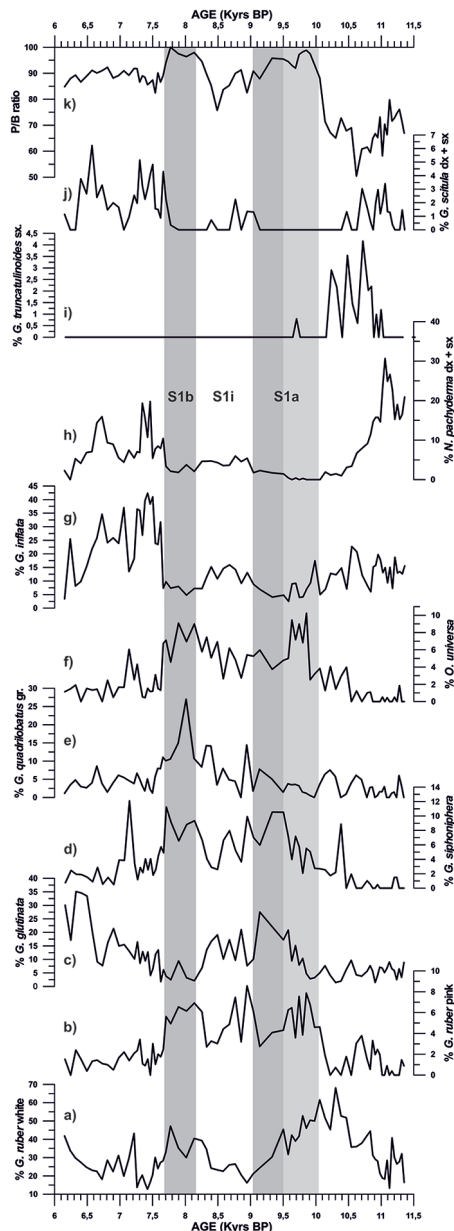
Figure 6. Records of planktonic foraminifera assemblages from core ND14Mbis for the 11.5–6 kyrs time interval. Grey bars represent the S1a and S1b phase time intervals, while light grey bar shows the subdivision of S1a.

Adriatic record (Siani et al., 2010) at 9 kyrs BP (Figure 3). However, for Geraga et al. (2008) this 500 yr discrepancy could be attributed to weak chronological constraints since the age model for this record has only one sample dated by radiocarbon during the sapropel event (Figure 3). These differences on the δ^{18}O$_{G.ruber}$ depletion age, between different cores (Ionian, Adriatic, and Aegean Sea), have already been described by other authors, who determined that the onset of the Sapropel layer deposition throughout the eastern Mediterranean Sea was not synchronous, irrespectively of the water depth deposition (10.8 ±0.4–6.1 ±0.5 Kyrs BP; De Lange et al., 2008; Incarbona et al., 2019). In spite of this asynchronicity, the similarities between the δ^{18}O data of the four cores confirm the consistency of the age model for our study core within the ^{14}C age uncertainty (Figure 3).

In the study core, the main planktonic foraminiferal change during this interval is the antithetic distribution patterns between *G. ruber* white and *N. pachyderma* (Figures 7a and c). In particular, *G. ruber* white, indicator of stratified (Principato et al., 2003), warm and oligotrophic surface waters (Hemleben et al., 1989;

Zaric et al., 2005), shows a progressive abundance increase during the pre-S1, reaching maximum values at 10.3 kyrs BP. This species is associated with the presence of *G. ruber* pink, strongly suggesting stratified surface water conditions. Conversely, *N. pachyderma*, a deep dweller cold-water species linked to winter/ spring high productivity and to a distinct deep chlorophyll maximum layer (Rohling and Gieskes, 1989), shows a decreasing abundance trend over the pre-S1 interval. This antithetic planktonic foraminiferal signature, previously documented in the Sicily Channel (Sprovieri et al., 2003), in the Gulf of Taranto (Di Donato et al., 2019), in the North eastern Ionian Sea (Geraga et al., 2008) and the Aegean Sea (Kontakiotis et al., 2009, 2013; Kontakiotis, 2016), suggests the gradual development of stratified and oligotrophic surface waters. In particular, high abundance of *N. pachyderma*, between 11.3 and 10.9 kyrs BP, suggests a well-developed deep Chlorophyll maximum and probably represents the end of the cooling related to the Younger Dryas event (i.e. Sprovieri et al., 2003; Di Donato et al., 2019). Upwards, peaks in abundance of *G. inflata* and *G. truncatulinoides* associated with *G. scitula* (Figures 6g, I, and j) suggest prevailing cool and deep vertical mixing conditions during winter (Hemleben et al., 1989; Pujol and Vergnaud-Grazzini, 1995). From 10.3 kyr BP, a sharp increase in the abundance of *G. ruber* white, associated with a sharp decrease of *G. inflata* and *G. truncatulinoides*, suggest the beginning of enhanced stratification of the water column. This micropaleontological signature is also associated with a gradual decrease in P/B ratio present both on our study core and on core MP50PC (Filippidi et al., 2016), located very close to our study area (North Ionian Sea), implying a progressive decrease in bottom waters oxygen concentration. According to these planktonic foraminiferal assemblages, we interpret the pre-Sapropel interval as a period with strong seasonality, having warm stratified surface water conditions but with winters characterized by colder waters and enhanced vertical mixing in the water column. The increased stratification could be the result of the entrance of freshwater and decreased surface water density. Plausible scenarios for the increased freshwater input suggest a combination of both postglacial freshening, with the entrance of a less salty inflow from the Atlantic waters, and the African monsoon, with the increase of the rivers inflow and precipitations (Casford et al., 2002; Cita et al., 1977; De Lange et al., 1999, 2008; Di Donato et al., 2019; Rohling 1994; Rohling et al., 1997, 2015).

Sapropel interval: S1a (10–9 kyrs BP)

The onset of S1a interval occurs at 10 kyrs BP and is marked by the disappearance of *G. truncatulinoides* (Geraga et al., 2008; Sprovieri et al., 2003). This S1a interval is also characterised by the increase in abundance of warm planktonic foraminiferal species (*G. ruber* pink, *G. quadrilobatus* gr. and *O. universa*) and the low abundance (or absence) of cold planktonic foraminiferal ones (*N. pachyderma, G. truncatulinoides, G. inflata* and *G. scitula*), suggesting a progressive stratification of the water column (Figure 6). One of the main planktonic foraminiferal features over the S1 deposition is the strong increase in abundance of *G. ruber* pink (Figure 7b). This feature has been previously documented by several authors (Casford et al., 2007; Geraga et al., 2008; Siani et al., 2010) in different areas of the eastern Mediterranean (south and north-east Ionian Sea, east of Crete Island, south Aegean Sea). In particular, our records show an evident replacement of *G. ruber* white distribution pattern by *G. ruber* pink from 10 to 9.5 kyrs BP (Figure 7a and b) indicating a possible sub-phase inside S1a. This ecological feature could suggest a shift from an oligotrophic environment to eutrophic conditions, related to the ecological preferences of these species to warm, stratified surface waters (Hemleben et al., 1989; Pujol and Vergnaud-Grazzini, 1995). High abundance values of *G. ruber* pink result in phase
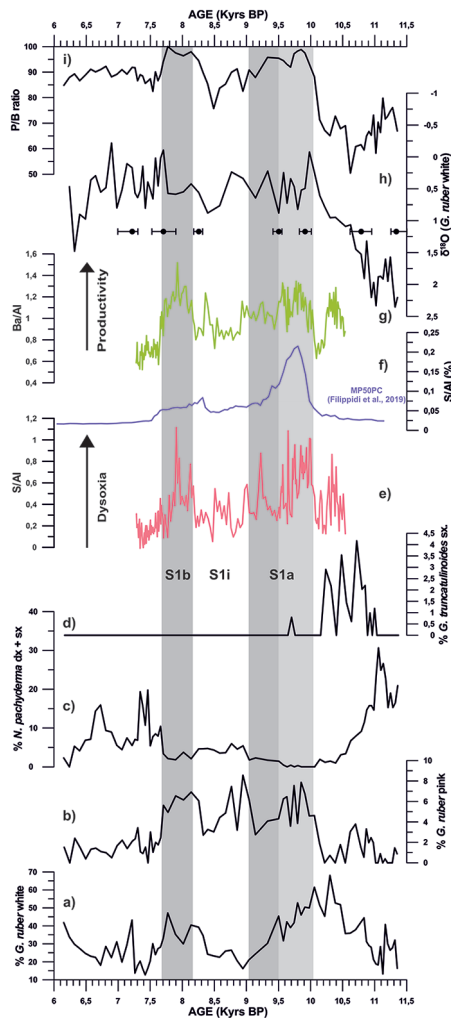
Figure 7. Records from core ND14Mbis of (a) *Globigerinoides ruber* white, (b) *Globigerinoides ruber* pink, (c) *Neogloboquadrina pachyderma*, (d) *Globorotalia truncatulinoides*, (e) Sulphur/Aluminium ratio (S/Al), (f) Sulphur/Aluminium ratio (S/Al) from core MP50PC (in purple, Filippidi et al., 2019), (g) Barium/Aluminium ratio (Ba/Al), (h) δ¹⁸O$_{G.ruber}$ data of core ND14Mbis (i) Planktonic/Benthic foraminifera ratio (P/B ratio). Grey bars represent the S1a and S1b phase time intervals, while light grey bar shows the subdivision of S1a.

with maximum Ba/Al values (Figures 7b and g). The Ba enrichment in sediments is also interpreted an increased productivity. In fact, Ba/Al ratio (Figure 7g), measured both in foraminiferal tests and bulk sediments (Antonarakou et al., 2015; Hönisch et al., 2011), is considered as paleo-productivity proxy (i.e. Gallego-Torres et al., 2007; Martínez-Ruiz et al., 2000). According to this latter Ba/Al interpretation and its agreement with the *G. ruber* pink record, we could confirm a high productivity interval between 10 and 9.5 kyr BP that we defined as the first sub-phase of S1a. The parallelism between *G. ruber* pink and Ba/Al record states a progressive decrease in productivity versus the end of S1a interval (9.5–9 kyr BP; second sub-phase of S1a). In this study, Ba/Al record is very similar to the ones on core MP50PC (north Ionian Sea) of Filippidi et al. (2016).

The opportunistic planktonic foraminiferal species *G. glutinata* shows low values during the beginning of S1a interval (average of 5%), however, from 9.5 to 9 kyrs BP (during the second sub-phase of S1a) presents an abrupt increase in abundance up to 27.5% (Figure 6c). This species is linked to a local rapid nutrient increase and is a specialist diatom feeder, thus being particularly abundant in areas with high continental runoff and high river input; this species can survive on a wide thermal range and within

the deep surface mixed layer (Hemleben et al., 1989). The concomitant increase in abundance of *G. glutinata* and *G. siphonifera* seems to suggest the shift at the end of S1a interval to relatively well-mixed water masses during the winter season (Rohling et al., 2004). We argue that during the second S1a sub-phase, the stratification of the water column might have decreased slightly, resulting in a replacement of *G. ruber* pink by *G. glutinata*, since this species has a wider range of adaptability.

The increase of P/B ratio during S1a (Figure 7i) suggests dysoxic conditions on the bottom waters, since these are not suitable conditions for the proliferation of benthic foraminiferal species. The low oxygen concentration in deep waters could be the result of high nutrient content during a time of surface water stratification. These conditions allowed to the organic matter to be transported downward in the water column and deposited. The respiration of this organic matter by bacteria together with reduced deep water ventilation as a result of the stratified surface waters eventually established the dysoxic conditions necessary to preserve the organic matter and therefore the formation of the Sapropel layer. We interpret the waters as being dysoxic and not anoxic because the benthic foraminiferal fauna (*Cassidulinoides brady*, *Gyroidina* spp., *Miliolids*, *Planulina ariminensis*, *Cibicides* spp., *Cibicidoides* spp. and *Planulina* spp.) does not completely disappear, being present in almost all the samples even if it is in low proportions (Figure 7i). This hypothesis is also supported by the similar P/B ratio in core MP50PC (Filippidi et al., 2016) and by the higher values shown by our S/Al record and in core MP50PC (Filippidi et al., 2016) during S1a (Figure 7e and f). Sulphur is attributed to pyrite formation that precipitates during reducing conditions (low oxygen) in the bottom waters (Filippidi et al., 2016). According to the P/B and S/Al ratios on both our core and on Filippidi et al. (2016), the second sub-phase of S1a (9.5–9 kyrs BP) was less dysoxic than the first one (10–9.5 kyrs BP), likely due to relatively less productivity than the first sub-phase (as described by *G. ruber* pink and Ba/Al) and less stratification (as described by *G. glutinata*).

Sapropel interruption: S1i (9–8.2 kyrs BP)

The main planktonic foraminiferal signature during the Sapropel interruption (S1i; 9–8.2 kyrs BP) is a general increase in abundance of the cold-water species *G. inflata* and *N. pachyderma*. The increase of these two species, indicative of a well-developed thick and cold mixed layers and formation of a deep chlorophyll maximum layer (Pujol and Vergnaud Grazzini, 1995) has been previously documented by several authors in the Eastern Mediterranean Basin (Casford et al., 2001; Geraga et al., 2008, 2010; Giamali et al., 2019; Kontakiotis et al., 2013; Kontakiotis, 2016; Lirer et al., 2013; Principato et al., 2003; Siani et al., 2010; Sprovieri et al., 2003; Triantaphyllou et al., 2009). The concomitant decrease in abundance of warm water planktonic foraminifera *G. ruber* white and *O. universa* with the slightly heavier values in δ¹⁸O *G. ruber* signal, describe the S1i as a relatively colder period. In addition, during this sapropel interruption (S1i) phase, the increase in benthic foraminiferal species, documented by a shift in P/B ratio, as also reported in Filippidi et al. (2016) in the Ionian Sea record, suggests an improvement of the bottom water conditions for the proliferation of those benthic species (Figure 7i). These planktonic and benthic foraminiferal signals document a re-ventilation of the deep waters linked to mixing processes, thus giving further arguments in favour of the possible entry of colder waters. These new paleoceanographic conditions are in agreement with the decrease in sulphur (S/Al, Figure 7e and f) signature during S1i, suggesting less pyrite formation, hence more oxygen content in the bottom waters, defining a partial re-oxygenation. The entry of these colder waters could have been at an intermediate depth, since the mixing had effects on both the surface and the deep waters. In addition, the

Ba/Al record show lower values suggesting a decreasing input of productivity (Figure 7g).

A peculiar planktonic foraminiferal feature, occurring during S1i interval, is the presence of *G. ruber* pink with a relative maximum peak at 8.9–8.7 kyrs BP. This signature has not been documented in any other Mediterranean cores and due to a lack of additional data, we have no further insight on why this feature appears on our core. Despite the cause being unknown and the lack of data to support our hypothesis, we can suggest a possible scenario for the appearance of this species during S1i. *G. ruber* pink variety occurs preferentially at the end of summer (Pujol and Vergnaud-Grazzini, 1995), thus the peak on our data could be interpreted as the result of seasonal resilient stratification that helped preserve warmer waters at a surface level. Core Z1 (Geraga et al., 2008) is located near our core but it does not present this feature, thus we interpret that this phenomenon must have been occurring very locally, and is not particular of whole Ionian Sea.

Sapropel interval: S1b (8.2–7.7 kyrs BP)

S1b interval (8.2–7.7 kyrs BP) is defined by an increase of warm planktonic foraminiferal species (i.e. *G. ruber* white, *G. ruber* pink, *G. quadrilobatus* gr. and *O. universa*) and a decrease of cold ones (i.e. *G. inflata* and *N. pachyderma*) (Figure 6). According to the increase in abundance of *G. ruber* pink (Figure 7b) and the increase in Ba/Al ratio (Figure 7g), S1b interval can be characterized by high nutrient content, also visible with the darker colour of the sapropel layer described by the lightness values (Figures 4a and 5a). The strong increase in abundance of *G. quadrilobatus* gr. and *O. universa*, over the S1b phase, as previously documented in the eastern Ionian Sea (Geraga et al., 2008), and the Aegean Sea (Giamali et al., 2019; Kontakiotis, 2016; Kontakiotis et al., 2013; Triantaphyllou et al., 2009), suggests the presence of an extended warm climate conditions and mixed layer during summer season (i.e. Pujol and Vergnaud Grazzini, 1995). In addition, the occurrence of *G. siphonifera*, might state well-mixed water masses during winter season (Rohling et al., 2004).

High values of the P/B ratio during S1b interval (comparable to Those of Filippidi et al., 2016), together with an increase of the S/Al record (Figures 7e, f, and i), suggest dysoxic bottom waters conditions, similar to that documented in the first sub-phase of S1a interval. In addition, we suggest that the main source area of nutrients over S1b interval was the increased river runoff, as stated during S1a, even if *G. glutinata* has very low abundance values. The high stratification of the water column during S1b, similar to that of the first sub-phase of S1a (as described by the P/B ratio and S/Al), could have allowed the proliferation of *G. ruber* pink not giving space to *G. glutinata* opportunistic species to occupy its biological niche. In fact, this antagonistic distribution pattern between *G. ruber* pink and *G. glutinata* characterize the entire sapropel event.

Post-Sapropel interval: post-S1 (post 7.7 kyrs BP)

From 7.7 kyr BP upwards (post-sapropel period), there is a strong and sudden recovery in the abundance of cold-water species (*G. inflata, N. pachyderma* and *G. scitula*) whereas the warm water ones (*G. ruber* white, *G. ruber* pink, *G. quadrilobatus* gr. and *O. universa*) describe an opposite trend (Figure 6). This abrupt change in the planktonic foraminiferal assemblage and the strong decrease in the Ba/Al records (similar to Filippidi et al., 2016) mark the end of the stagnation and high productivity period, therefore ending S1 (Figure 7g), marking the onset of the re-establishment of cool water conditions and vertical mixing during the winter. The P/B ratio (Figure 7i) associated with the depletion in S/Al signal (Figures 7e and f) shows values similar to that documented during the Sapropel S1i and it never recovers the well-oxygenated deep water

conditions as during the pre-Sapropel deposition. In addition, a strong increase in Mn/Al ratio at 7.8 kyrs BP (Figure 5d), marks the occurrence of the manganese marker layer, a well-documented layer of variable thickness (between 2–3 cm) that overlies most sapropel layers in the eastern Mediterranean Sea (De Lange et al., 1999; Filippidi and De Lange, 2019; Martinez-Ruiz et al., 2000; Mercone et al., 2000; Meier et al., 2004; Thomson et al., 1999). This Mn-rich layer has a light dark colour characteristic from sediments enriched with Mn and a 2 cm thickness, a diffuse upper boundary and a relatively abrupt colour transition at its lower boundary (Figure 2a). It was formed when, after the sapropel event, the dysoxic deep waters were re-ventilated, since Mn is present in the soluble form under dysoxic conditions but it precipitates when oxygen is added (Martinez-Ruiz et al., 2000; Meier et al., 2004; Thomson et al., 1995, 1999), thus additional Mn peaks can be found.

Conclusion

We present a high-resolution paleoceanographic reconstruction based on a multi-proxy approach of the most recent sapropel event (S1) (10–7.7 kyrs BP) in a 655 m water depth record from the North Ionian Sea (eastern Mediterranean Sea). The ecological interpretation of planktonic foraminiferal assemblages, integrated with the XRF elemental data and oxygen isotope *G. ruber* record have provided an accurate interpretation of the changes in surface water properties. The results allowed us to divide S1 into different phases, starting with a preconditioning period (pre-S1) from 11.3 to 10 kyrs BP. We define the pre-S1 as a period with strong seasonality, having warm stratified surface water conditions but with colder winters characterized by an intensification of vertical mixing in the water column. A progressive increase of P/B ratio also suggests a depletion of oxygen concentration of the bottom water. Later, S1 interval has been divided into two warm phases, S1a (10–9 kyrs BP) and S1b (8.2–7.7 kyrs BP), separated by a cold interruption event, S1i (9–8.2 kyrs BP). Proxies of paleo-productivity (*G. ruber* pink and Ba/Al) and proxies linked to mixing of the water column (*G. ruber* white and *N. pachyderma*) indicate that S1a and S1b were characterized by stratified surface waters rich in nutrient content. The deposition of S1a started at 10 kyrs BP with an increase in nutrients related to the river runoff. P/B ratio and S/Al records allowed to define S1a and S1b as dysoxic events. The interruption of S1 (S1i) is characterized by the entrance of colder waters that caused mixing of the stratified water column and re-ventilated of the deep dysoxic waters. The high resolution of our record allowed the identification of a two sub-phases into the S1a interval, being the first sub-phase (10–9.5 kyrs BP) characterized by high productivity, strong stratification and dysoxic deep waters, while the second sub-phase (9.5–9 kyrs BP) by less productivity and a slightly decreased level of stratification that caused less dysoxic deep waters. We conclude that S1 was the result of a complex interaction of different oceanographic processes triggered by the arrival of fresh nutrient-rich waters that caused dysoxia on the deep ocean waters.

ORCID iD

Helena Checa [iD] https://orcid.org/0000-0002-6790-0957

References

Abu-Zied RH, Rohling EJ, Jorissen FJ et al. (2008) Benthic foraminiferal response to changes in bottom-water oxygenation and organic carbon flux in the eastern Mediterranean during LGM to Recent times. *Marine Micropaleontology* 67(1): 46–68.

Antonarakou A, Kontakiotis G, Mortyn PG et al. (2015) Biotic and geochemical (δ18O, δ13C, Mg/Ca, Ba/Ca) responses of Globigerinoides ruber morphotypes to upper water column variations during the last deglaciation, Gulf of Mexico. *Geochimica et Cosmochimica Acta* 170: 69–93.

Antonarakou A, Kontakiotis G, Karageorgis AP et al. (2019) Eco-biostratigraphic advances on late Quaternary geochronology and paleoclimate: The marginal Gulf of Mexico analogue. *Geological Quarterly* 63(1): 178–191.

Antonarakou A, Kontakiotis G, Zarkogiannis S et al. (2018) Planktonic foraminiferal abnormalities in coastal and open marine eastern Mediterranean environments: A natural stress monitoring approach in recent and early Holocene marine systems. *Journal of Marine Systems* 181: 63–78.

Bazzicalupo P, Maiorano P, Girone A et al. (2020) Holocene climate variability of the Western Mediterranean: Surface water dynamics inferred from calcareous plankton assemblages. *The Holocene* 30(5): 691–708.

Blaauw M and Christen JA (2011) Flexible paleoclimate age-depth models using an autoregressive gamma process. *Bayesian Analysis* 6(3): 457–474.

Cacho I, Grimalt JO, Canals M et al. (2001) Variability of the western Mediterranean Sea surface temperature during the last 25,000 years and its connection with the Northern Hemisphere climatic changes. *Paleoceanography* 16(1): 40–52.

Calvert SE and Fontugne MR (2001) On the late Pleistocene-Holocene Sapropel record of climatic and oceanographic variability in the eastern Mediterranean. *Paleoceanography* 16(1): 78–94.

Calvert SE and Pedersen TF (2007) Chapter fourteen elemental proxies for palaeoclimatic and palaeoceanographic variability in marine sediments: Interpretation and application. *Developments in Marine Geology* 1: 567–644.

Casford JSL, Abu-Zied R, Rohling EJ et al. (2007) A stratigraphically controlled multiproxy chronostratigraphy for the eastern Mediterranean. *Paleoceanography* 22(4): 4215.

Casford JSL, Rohling EJ, Abu-Zied R et al. (2002) Circulation changes and nutrient concentrations in the Late Quaternary Aegean Sea: A non-steady state concept for Sapropel formation. *Paleoceanography* 17(2): 14–1.

Casford JSL, Rohling EJ, Abu-Zied RH et al. (2003) A dynamic concept for eastern Mediterranean circulation and oxygenation during sapropel formation. *Palaeogeography, Palaeoclimatology, Palaeoecology* 190: 103–119.

Cita M, Vergnaud-Grazzini C, Robert C et al. (1977) Paleoclimatic record of a long deep sea core from the Eastern Mediterranean. *Quaternary Research* 8(2): 205–235.

Coplen TB (1996) New guidelines for the reporting of stable hydrogen, carbon, and oxygen isotope ratio data. *Geochimica et Cosmochimica Acta* 60(17): 3359–3360.

Cornuault M, Tachikawa K, Vidal L et al. (2018) Circulation changes in the Eastern Mediterranean Sea over the past 23,000 years inferred from authigenic Nd isotopic ratios. *Paleoceanography and Paleoclimatology* 33(3): 264–280.

Cushman-Roisin B, Gacic M, Poulain PM et al. (2001) *Physical Oceanography of the Adriatic Sea: Past, Present and Future*. Leeds: Springer-Science + Business Media, BV.

Di Donato V, Insinga DD, Iorio M et al. (2019) The palaeoclimatic and palaeoceanographic history of the Gulf of Taranto (Mediterranean Sea) in the last 15 ky. *Global and Planetary Change* 172: 278–297.

De Lange GJ, Thomson J, Reitz A et al. (2008) Synchronous basin-wide formation and redox-controlled preservation of a Mediterranean Sapropel. *Nature Geoscience* 1(9): 606–610.

De Lange GJ, Van Santvoort PJM, Langereis C et al. (1999) Paleo-environmental variations in eastern Mediterranean sediments: A multidisciplinary approach in a prehistoric setting. *Progress in Oceanography* 44(1–3): 369–386.

De Rijk S, Hayes A and Rohling EJ (1999) Eastern Mediterranean sapropel S1 interruption: An expression of the onset of climatic deterioration around 7 ka BP. *Marine Geology* 153(1–4): 337–343.

Drinia H, Antonarakou A, Tsourou T et al. (2016) Foraminifera eco-biostratigraphy of the southern Evoikos outer shelf, central Aegean Sea, during MIS 5 to present. *Continental Shelf Research* 126: 36–49.

Filippidi A and De Lange GJ (2019) Eastern Mediterranean deep water formation during sapropel S1: A reconstruction using geochemical records along a bathymetric transect in the Adriatic outflow region. *Paleoceanography and Paleoclimatology* 34(3): 409–429.

Filippidi A, Triantaphyllou MV and De Lange GJ (2016) Eastern-Mediterranean ventilation variability during Sapropel S1 formation, evaluated at two sites influenced by deep-water formation from Adriatic and Aegean Seas. *Quaternary Science Reviews* 144: 95–106.

Freeman E, Skinner LC, Reimer R et al. (2016) Graphitization of small carbonate samples for paleoceanographic research at the godwin radiocarbon laboratory, University of Cambridge. *Radiocarbon* 58(1): 89–97.

Gallego-Torres D, Martínez-Ruiz F, Paytan A et al. (2007) Pliocene–Holocene evolution of depositional conditions in the eastern Mediterranean: Role of anoxia vs productivity at time of Sapropel deposition. *Palaeogeography, Palaeoclimatology, Palaeoecology* 246(2–4): 424–439.

Garcia-Solsona E, Pena LD, Paredes E et al. (2020) Rare Earth Elements and Nd isotopes as tracers of modern ocean circulation in the central Mediterranean Sea. *Progress in oceanography* 185: 102340.

Geraga M, Ioakim C, Lykousis V et al. (2010) The high-resolution palaeoclimatic and palaeoceanographic history of the last 24,000 years in the central Aegean Sea, Greece. *Palaeogeography Palaeoclimatology Palaeoecology* 287(1–4): 101–115.

Geraga M, Mylona G, Tsaila-Monopoli St et al. (2008) Northeastern Ionian Sea: Paleoceanographic variability over the last 22 ka. *Journal of Marine Systems* 74(1–2): 623–638.

Giamali C, Koskeridou E, Antonarakou A et al. (2019) Multiproxy ecosystem response of abrupt Holocene climatic changes in

the north-eastern Mediterranean sedimentary archive and hydrologic regime. *Quaternary Research* 92(3): 665–685.

Grant KM, Grimm R, Mikolajewicz U et al. (2016) The timing of Mediterranean sapropel deposition relative to insolation, sea-level and African monsoon changes. *Quaternary Science Reviews* 140: 125–141.

Grimm R, Maier-Reimer E, Mikolajewicz U et al. (2015) Late glacial initiation of Holocene eastern Mediterranean Sapropel formation. *Nature Communications* 6(1): 1–12.

Hemleben Ch, Spindler M and Anderson OR (1989) *Modern Planktonic Foraminifera*. Leeds: Springer- Verlag.

Hennekam R, Jilbert T, Schnetger B et al. (2014) Solar forcing of Nile discharge and sapropel S1 formation in the early to middle Holocene eastern Mediterranean. *Paleoceanography* 29(5): 343–356.

Hönisch B, Allen KA, Russell AD et al. (2011) Planktic foraminifers as recorders of seawater Ba/Ca. *Marine Micropaleontology* 79(1–2): 52–57.

Incarbona A, Abu-Zied RH, Rohling EJ et al. (2019) Reventilation episodes during the sapropel S1 deposition in the Eastern Mediterranean based on holococcolith preservation. *Paleoceanography and Paleoclimatology* 34(10): 1597–1609.

Kallel N, Duplessy JC, Labeyrie L et al. (2000) Mediterranean pluvial periods and Sapropel formation over the last 200.000 years. *Palaeogeography, Palaeoclimatology, Palaeoecology* 157(1–2): 45–58.

Klein B, Wolfgang R, Civitarese G et al. (2000) Is the Adriatic returning to dominate the production of Eastern Mediterranean Deep Water? *Geophysical Research letters* 27(20): 3377–3380.

Kontakiotis G (2016) Late Quaternary paleoenvironmental reconstruction and paleoclimatic implications of the Aegean Sea (eastern Mediterranean) based on paleoceanographic indexes and stable isotopes. *Quaternary International* 401: 28–42.

Kontakiotis G, Antonarakou A and Zachariasse WJ (2013) Late Quaternary palaeoenvironmental changes in the Aegean Sea: Interrelations and interactions between North and South Aegean Sea. *Bulletin of the Geological Society of Greece* 47(1): 167–177.

Kontakiotis G, Antonarakou A, Mortyn PG et al. (2017) Morphological recognition of Globigerinoides ruber morphotypes and their susceptibility to diagenetic alteration in the eastern Mediterranean Sea. *Journal of Marine Systems* 174: 12–24.

Kontakiotis G, Antonarakou A, Triantaphyllou MV et al. (2009) Planktonic foraminiferal Mg/Ca as a proxy for paleoceanographic reconstruction during deposition of Holocene S1 sapropel in Aegean Sea. *Proceedings of 9th Symposium on Oceanography and Fishery* 1: 73–78.

Kotthoff U, Pross J, Müller UC et al. (2008) Climate dynamics in the borderlands of the Aegean Sea during formation of sapropel S1 deduced from a marine pollen record. *Quaternary Science Reviews* 27(7–8): 832–845.

Koutrouli A, Anastasakis G, Kontakiotis G et al. (2018) The early to mid-Holocene marine tephrostratigraphic record in the Nisyros-Yali-Kos volcanic center, SE Aegean Sea. *Journal of Volcanology and Geothermal Research* 366: 96–111.

Le Houedec S, Mojtahid M, Bicchi E et al. (2020) Suborbital hydrological variability inferred from coupled benthic and planktic foraminiferal-based proxies in the south-eastern Mediterranean during the last 19 ka. *Paleoceanography and Paleoclimatology* 35(2): e2019PA003827.

Lirer F, Sprovieri M, Ferraro L et al. (2013) Integrated stratigraphy for the Late Quaternary in the eastern Tyrrhenian Sea. *Quaternary International* 292: 71–85.

Louvari MA, Drinia H, Kontakiotis G et al. (2019) Impact of latest-glacial to Holocene sea-level oscillations on central Aegean shelf ecosystems: A benthic foraminiferal palaeoenvironmental assessment of South Evoikos Gulf, Greece. *Journal of Marine System* 199: 103181.

Manca BB, Budillon G, Scarazzato P et al. (2003) Evolution of dynamics in the eastern Mediterranean affecting water mass structures and properties in the Ionian and Adriatic Seas. *Journal of Geophysical Research* 108(C9): 8102.

Margaritelli G, Cisneros M, Cacho I et al. (2018) Climatic variability over the last 3000 years in the central – western Mediterranean Sea (Menorca basin) detected by planktonic foraminifera and stable isotope records. *Global and Planetary Change* 169: 179–187.

Marino G, Rohling EJ, Sangiorgi F et al. (2009) Early and middle Holocene in the Aegean Sea: Interplay between high and low latitude climate variability. *Quaternary Science Reviews* 28(27): 3246–3262.

Martinez-Ruiz F, Kastner M, Paytan A et al. (2000) Geochemical evidence for enhanced productivity during S1 Sapropel deposition in the eastern Mediterranean. *Paleoceanography* 15(2): 200–209.

Mélières MA, Rossignol-Strick M and Malaizé B (1997) Relation between low latitude insolation and δ18O change of atmospheric oxygen for the last 200 kyrs, as revealed by Mediterranean Sapropels. *Geophysical Research Letters* 24(10): 1235–1238.

Meier KJS, Zonneveld KAF, Kasten S et al. (2004) Different nutrient sources forcing increased productivity during eastern Mediterranean S1 Sapropel formation as reflected by calcareous dinoflagellate cysts. *Paleoceanography* 19(1): PA1012.

Mercone D, Thomson J, Abu-Zied RH et al. (2001) High resolution geochemical and micro-palaeontological profiling of the most recent eastern Mediterranean Sapropel. *Marine Geology* 177(1–2): 25–44.

Mercone D, Thomson J, Croudace IW et al. (2000) Duration of S1, the most recent sapropel in the eastern Mediterranean Sea, as indicated by accelerator mass spectrometry radiocarbon and geochemical evidence. *Paleoceanography* 15(3): 336–347.

Mojtahid M, Hennekam R, De Nooijer LJ et al. (2019) Evaluation and application of foraminiferal Element/Calcium ratios: Assessing riverine fluxes and environmental conditions during sapropel S1 in the south-eastern Mediterranean. *Marine Micropaleontology* 153: 101783.

Myers PG and Rohling EJ (2000) Modelling a 200-yr interruption of the Holocene sapropel S1. *Quaternary Research* 53(1): 98–104.

Özsoy E, Hecht A and Ünlüata Ü (1989) Circulation and hydrography of the Levantine Basin. Results of POEM coordinated experiments 1985–1986. *Progress in Oceanography* 22(2): 125–170.

Plancq J, Grossi V, Pittet B et al. (2015) Multi-proxy constraints on sapropel formation during the late Pliocene of central Mediterranean (southwest Sicily). *Earth and Planetary Science Letters* 420: 30–44.

Principato MS, Giunta S, Corselli C et al. (2003) Late Pleistocene–Holocene planktonic assemblages in three box-cores from the Mediterranean Ridge area (west-southwest of Crete): Palaeocological and palaeoceanographic reconstruction of sapropel S1 interval. *Palaeogeography, Palaeoclimatology, Palaeoecology* 190: 61–77.

Pujol C and Vergnuad-Grazzini C (1995) Distribution patterns of live planktic foraminifers as related to regional hydrography and productive systems of the Mediterranean Sea. *Marine Micropaleontology* 25(2–3): 187–217.

Reimer PJ, Bard E, Bayliss A et al. (2013) IntCal13 and Marine13 radiocarbon age calibration curves 0-50,000 years cal BP. *Radiocarbon* 55(4): 1869–1887.

Rohling EJ (1994) Review and new aspects concerning the formation of eastern Mediterranean sapropels. *Marine Geology* 122(1–2): 1–28.

Rohling EJ, Abu-Zied R, Casford JSL et al. (2009) *The Physical Geography of the Mediterranean*. Leeds: Oxford University Press.

Rohling EJ and Gieske WWC (1989) Late Quaternary changes in Mediterranean Intermediate Water density and formation rate. *Paleoceanography* 4(5): 531–545.

Rohling EJ and Pälike H (2005) Centennial-scale climate cooling with a sudden cold event around 8,200 years ago. *Nature* 434(7036): 975–979.

Rohling EJ, Jorissen FJ and De Stigter HC (1997) 200 year interruption of Holocene sapropel formation in the Adriatic Sea. *Journal of Micropaleontology* 16(2): 97–108.

Rohling EJ, Marino G and Grant KM (2015) Mediterranean climate and oceanography, and the periodic development of anoxic events (sapropels). *Earth-Science Reviews* 143: 62–97.

Rohling EJ, Mayewski PA, Abu-Zied RH et al. (2002) Holocene atmosphere-ocean interactions: Records from Greenland and the Aegean Sea. *Climate Dynamics* 18: 587–593.

Rohling EJ, Sprovieri M, Cane T et al. (2004) Reconstructing past planktic foraminiferal habitats using stable isotope data: A case history for Mediterranean sapropel S5. *Marine Micropaleontology* 50(1–2): 89–123.

Roussakis G, Karageorgis AP, Conispoliatis N et al. (2004) Last glacial-Holocene sediment sequences in N. Aegean basins: structure, accumulation rates and clay mineral distribution. *Geo-Marine Letters* 24(2): 97–111.

Schmiedl G, Kuhnt T, Ehrmann W et al. (2010) Climatic forcing of eastern Mediterranean deep-water formation and benthic ecosystems during the past 22000 years. *Quaternary Science Reviews* 29(23–24): 3006–3020.

Siani G, Paterne M and Colin Ch (2010) Late glacial to Holocene planktic foraminifera bioevents and climatic record in the South Adriatic Sea. *Journal of Quaternary Science* 25(5): 808–821.

Sprovieri R, Di Stefano E, Incarbona A et al. (2003) A high-resolution record of the last deglaciation in the Sicily Channel based on foraminifera and calcareous nannofossil quantitative distribution. *Palaeogeography, Palaeoclimatology, Palaeoecology* 202(1–2): 119–142.

Tachikawa K, Vidal L, Cornuault M et al. (2015) Eastern Mediterranean Sea circulation inferred from the conditions of S1 sapropel deposition. *Climate of the Past* 11(6): 855–867.

Tesi T, Asioli A, Minisini D et al. (2017) Large-scale response of the Eastern Mediterranean thermohaline circulation to African monsoon intensification during Sapropel S1 formation. *Quaternary Science Reviews* 159: 139–154.

Thomson J, Higgs NC, Wilson TRS et al. (1995) Redistribution and geochemical behaviour of redox-sensitive elements around S1, the most recent eastern Mediterranean sapropel. *Geochimica et Cosmochimica Acta* 59 (17): 3487–3501.

Thomson J, Mercone D, De Lange GJ et al. (1999) Review of recent advances in the interpretation of eastern Mediterranean sapropel S1 from geochemical evidence. *Marine Geology* 153(1–4): 77–89.

Triantaphyllou MV, Antonarakou A, Kouli K et al. (2009) Late Glacial-Holocene ecostratigraphy of the south-eastern Aegean Sea, based on plankton and pollen assemblages. *Geo-Marine Letters* 29(4): 249–267.

Vadsaria T, Ramstein G, Dutay JC et al. (2019) Simulating the occurrence of the last sapropel event (S1): Mediterranean basin ocean dynamics simulations using Nd isotopic composition modelling. *Paleoceanography Paleoclimatology* 34(2): 237–251.

Walker MJC, Head MJ, Berkelhammer M et al. (2018) Formal ratification of the subdivision of the Holocene Series/Epoch (Quaternary System/Period): Two new Global Boundary Stratotype Sections and Points (GSSPs) and three new stages/subseries. *Episodes* 41(4): 213–223.

Zaric S, Donner B, Fischer G et al. (2005) Sensitivity of planktic foraminifera to sea surface temperature and export production as derived from sediment trap data. *Marine Micropaleontology* 55(1–2):75–105.